ACS OMEGA

Open Access

http://pubs.acs.org/journal/acsodf

Article

Could the Rebound Characteristics of Oblique Impact for SiO_2 Particles Represent the Ash Particles?

Xue Li, Jun Xie,* Ming Dong, Sheng Chen, and Wenjie Dong

Cite This: *ACS Omega* 2024, 9, 10459−10467

Read Online

ACCESS | Metrics & More | Article Recommendations | Supporting Information

ABSTRACT: Collisions between particles or with a surface have been widely applied, in which the restitution coefficients are the important parameter to describe the particle rebound behavior. SiO_2 particles are often used instead of ash particles in theoretical analyses; however, whether this is justifiable has not been confirmed. This paper compares the rebound characteristics of oblique impact for SiO_2 particles and ash particles by experimental and theoretical analyses. Based on the rigid-body theory, the tangential restitution coefficients, rebound angle-particle center, and reflection angle-contact path predicted by SiO_2 particles are basically in agreement with the experimental results for ash particles, especially at large impact angles. However, there is a slight error at 2.2 m/s as the velocity approaches the critical capture velocity.

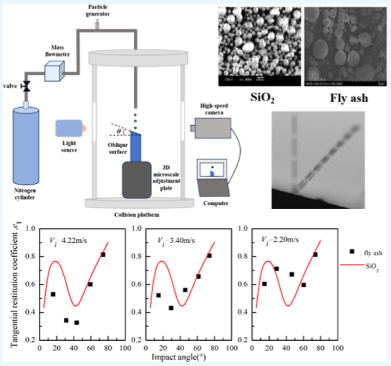

1. INTRODUCTION

In the chemical and steel industry, coal is the main energy for production. Ash, as a combustion product of coal, constitutes a primary influencing factor on the heat transfer efficiency of the heat exchanger and causes environmental pollution. The ash deposition on the heat transfer surfaces is one of the primary problems relevant to pulverized coal boiler operation and design and fuel selection.[1−3] It has been reported that excess ash deposition in convective coolers not only leads to unplanned shutdowns but also causes a reduction in heat transfer or even causes the corrosion of the boiler heat exchange tube.[4] Therefore, it is necessary to control the ash deposition. This led to advances in developing models to predict ash deposition behavior.

The impact between a sphere and a substrate is one of the basis mechanisms in the formation of ash deposition, especially the restitution coefficient of the impact is a relevant boundary condition that defines the particle fate within computational fluid dynamics models for predicting the ash deposition process.[5−7] There are many factors that influenced the impact results, such as the particle velocity, impact angle, particle radius, particle shape, property parameters of the particle and surface, reaction atmosphere, coal type, flow dynamics, and so on.[8−11] Many researchers have intensively investigated the particle impact through experiments and proposed many models to predict the rebound behaviors of the particle.

One of the earliest experiments that show the direct measurement of particle velocity for normal impact under vacuum conditions was conducted by Dahneke.[12] The restitution coefficient for normal impact was presented, and the critical capture velocity that occurs when the particle motion stops upon impact with a surface was discovered; however, its accurate value was not achieved in those work. In order to obtain the accurate value, Rogers and Reed[13] measured the critical capture velocities of the impact for glass, copper, and stainless-steel particles with a high-speed camera. The effect of the particle material on the critical capture velocity was achieved. For other factors, Wall et al.[14] researched the effect of particle diameters, particle and surface material, and impact velocity on critical capture velocity by experiments. Furthermore, the process of particle energy change and the normal restitution coefficient under different collision conditions were investigated.

For oblique impacts, tangential force causes sliding or localized slip, which modifies the rebound characteristic of particles. Researchers found that particles can still bounce when the normal incident velocity was less than the critical capture velocity.[15,16] The effect of impact angle on normal restitution coefficient (e_n), tangential restitution coefficient (e_t), and total restitution coefficient (e) had been researched by experimental and theoretical methods.[10] It was found that e_n fluctuates little with the impact angle, while e_t varies greatly. A classical rigid-body theory based on the impulse theorem and the momentum theorem was developed to predict the particle rebound characteristics.[17] According to the classical rigid-body

Received: October 28, 2023
Revised: February 8, 2024
Accepted: February 14, 2024
Published: February 22, 2024

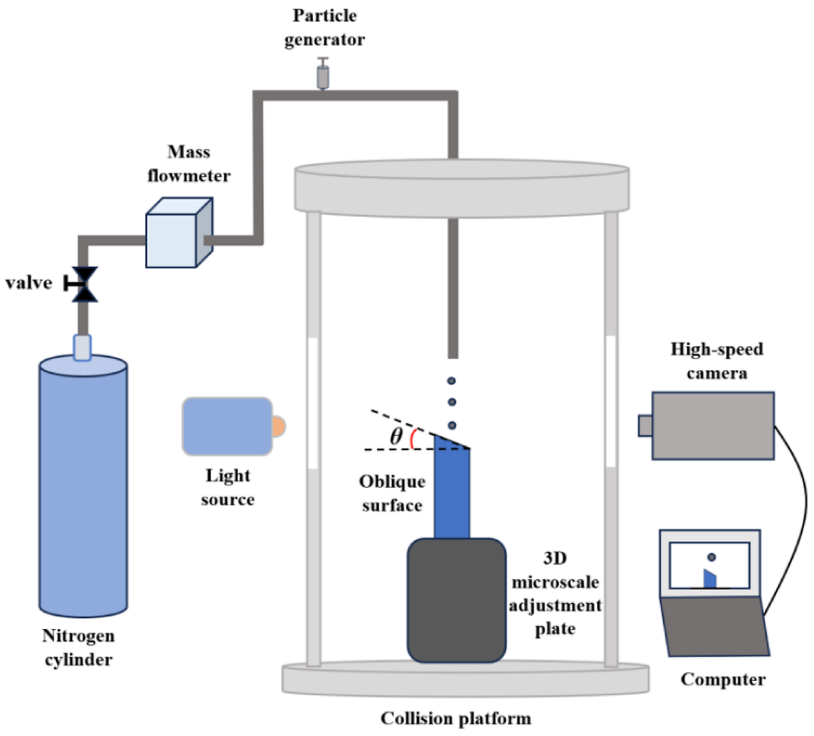

Figure 1. Experimental system of particle oblique impact.

theory, Wu et al.[18,19] analyzed the particle motions after the elastoplastic particles obliquely impact the elastoplastic surface by the finite element method and propose a dimensionless analysis method to predict e_t, with e_n. Based on the dimensionless analysis method, Tomar and Bose[20] compared the restitution coefficient of glass and steel particles with diameters between 1 and 6 mm. It was found that e_t is a function of e_n and impact angle; sticking occurs at larger impact angles, while sliding dominates at lower impact angles. During elastic collision, the critical impact angle that distinguishes between sticking and sliding is determined by Maw et al. and a method for deriving the coefficient of sliding friction was obtained.[21,22]

For real ash particles, the rebound parameters are different to predict due to multiple factors affecting the collision process, for example, carbon conversion, temperature, impact velocity, surface properties, and structure.[23,24] A 2D model was developed to predict the rebound characteristic of ash particles in the boiler.[25,26] Research found that the shape and size of ash particles are practical reasons for deposition. Yang et al.[27] considered the influence of impact angle, incident velocity, particle properties, and furnace operation conditions on particle deposition. The maximum deposition efficiency approaches that of small particles with an increased incidence velocity. For near-wall studies, Troiano et al.[28,29] carried out experiments on oblique impact of coal, char, and ash particles with a flat surface. The effect of carbon conversion, impact velocity, and surface properties on the restitution coefficient had been investigated. They also pointed out that the particle material and the surface properties have little effect on e_n during oblique collision. The variation of the restitution coefficient of ash particles with the impact angle and incident velocity has been obtained experimentally.[30,31] However, the above studies quantitatively describe only the rebound parameters of ash particles. Compared to ash particles, the rebound behavior of SiO_2 particles with a regular single property are easier to obtain. Therefore, it is more meaningful to predict the rebound characteristics of ash particles by SiO_2 particles.

Above all, the experimental and theoretical investigations of SiO_2 particles and ash particles that obliquely impact the stainless-steel surface are presented. The variations of restitution coefficient, rebound angle, and dynamic friction coefficient are determined by experiments. The emphasis is on using the rebound parameter from regular SiO_2 particles to predict ash particles' behavior after oblique impact with a surface. Based on the rigid-body theory, the rebound angle velocities and tangential restitution coefficients of SiO_2 particles were obtained, and the rebound parameters of ash particles were further predicted.

2. EXPERIMENTAL SYSTEM

The experimental facility for the oblique impact between the particle and stainless-steel plate is shown in Figure 1. The experimental facility mainly includes the inlet system, a collision unit, and a high-speed camera system. The nitrogen as the transport gas drives the particles into the collision unit. The airflow is adjusted by the mass flow meter and consequently changes the particle incident velocity. The particle is injected using a particle generator. The surface roughness of the stainless-steel plate is kept below 0.2 μm. The surface inclination angle varies from 15 to 75° at an interval of 15°. The high-speed camera system consists of a light source and a Phantom v12.1 digital high-speed camera with a 10× lens and a computer. The captured particles are in the focus plane of the camera for high-resolution images. The shooting parameters of the digital high-speed camera are shown in Table 1. The time interval of particle images in Figure S1 was two frames. The incident velocity of the SiO_2 particle was 4.23 m/s with an impact angle of 15°.

https://doi.org/10.1021/acsomega.3c08519
ACS Omega 2024, 9, 10459−10467

Table 1. Technology Parameters of Phantom v12.1

item	parameter
lens	VS-M0910 M × 10 microscopic
frame rate	66,037 frames/s
exposure time	6.22 μs
resolution	256 × 256

To ensure the accuracy of the experiment, no less than 30 experimental groups are conducted at the same condition. The incident and rebound velocities of the particles are obtained by averaging the velocities between the captured images of the particle before and after the collision. During high-speed camera shooting, the random error of the sampling is ±0.5%, and the position uncertainty of the particle in the image is ±l pixel. Therefore, the measured mean displacement error is ±0.5 pixel. In this experiment, the random error is 0.38 at a 4.3 m/s incident velocity, and the relative error is ±8.8%. The deviations of the impact angle and particle diameter are ±1.5° and ±2.75 μm, respectively.

The deposition of ash particles on the heat exchanger surface is the main factor affecting the heat exchange efficiency in the boiler heat exchanger. The majority of the ash deposition on the heat exchange surface is from the inertial impaction of particles with diameters larger than 10 μm.[32] For different types of coal, the ash content varies. The predominant component in the ash is always SiO_2.[33,34] Therefore, the SiO_2 and ash particles with diameters of 25 μm are selected. The morphology of the SiO_2 particle is obtained by SEM, as shown in Figure 2. The diameter distribution of the SiO_2 particle in Figure S2 is measured by a laser particle size analyzer (Mastersizer 2000, Malvern Instruments Ltd., Malvern, UK). The ash particles used in this study were from an actual power plant, as imaged by SEM in Figure 3. The bulk of the diameters is in the range of 5−30 μm. A particle size of 25 μm was selected for both SiO_2 and ash particles in the experiment.

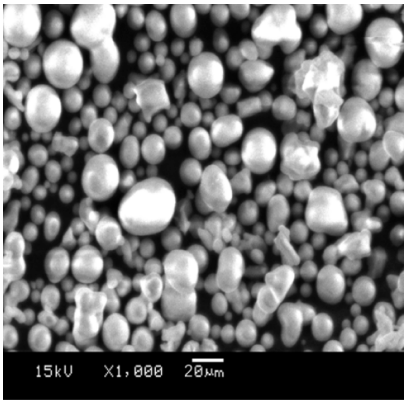

Figure 2. Morphology of SiO_2 particles imaged by SEM.

This article assumes that the crystalline phase of ash only consists of quartz and mullite. Through XRD analysis, the density and Young's modulus of ash particles are calculated as follows, and the results are listed in Table 2.

$$\rho_{\text{fly ash}} = \rho_g V_g + \rho_m V_m + \rho_q V_q \quad (1)$$

$$E_{\text{fly ash}} = E_g V_g + E_m V_m + E_q V_q \quad (2)$$

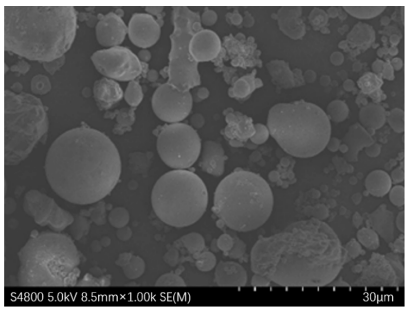

Figure 3. Ash particle imaged by SEM.

Table 2. Physical Parameters of Ash Particles Are Derived by XRD

item	total crystalline phase	quartz	mullite	ash	SiO_2
ratio %	44.90	6.80	38.10		
density (kg/m^3)	2500	2650	2800	2370	2320
Young's modulus (GPa)	73	94	230	127	75

where ρ is the density, E is the Young's modulus, V is the volume fraction, and subscripts g, q, and m denote glass, quartz, and mullite, respectively.

3. THEORETICAL CONSIDERATIONS

The schematic of the particle oblique impact with the surface is shown in Figure 4. Note that V, v, and w are the velocities of the sphere center, the translational velocities at the contact path, and the angular velocities, respectively. The subscripts i and r indicate the incidence and rebound phases, respectively.

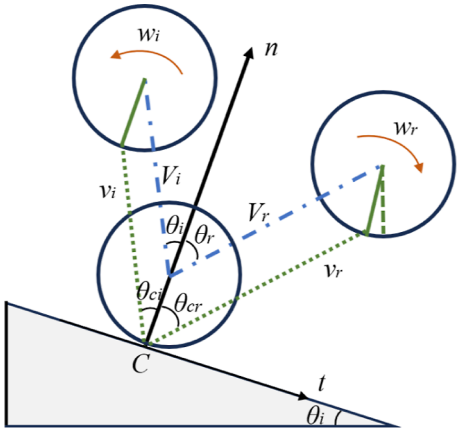

Figure 4. Schematic of the particle obliquely impacting the surface.

As the particle obliquely impacts with stainless-steel plate, e_n, e_t, and e are given by

$$e_n = \frac{V_{nr}}{V_{ni}} \quad (3)$$

$$e_t = \frac{V_{tr}}{V_{ti}} \quad (4)$$

$$e = \frac{V_r}{V_i} = \sqrt{e_n^2 \cos^2 \theta_i + e_t^2 \sin^2 \theta_i} \quad (5)$$

https://doi.org/10.1021/acsomega.3c08519
ACS Omega 2024, 9, 10459−10467

where θ_i is the impact angle and the subscripts n and t represent normal and tangential directions, respectively.

The impulse ratio is used to describe the correlation between the tangential and normal interactions during an impact. According to Newton's second law and the conservation of angular momentum about point C, the impulse ratio f, normal impulse P_n, the tangential impulse P_t, and the angular momentum P_w are as follows

$$f = \frac{P_t}{P_n} \tag{6}$$

$$P_n = m(V_{ni} + V_{nr}) \tag{7}$$

$$P_t = m(V_{ti} - V_{tr}) \tag{8}$$

$$P_w = I(\omega_i - \omega_r) = RP_t \tag{9}$$

where m, I, and ω are the particle quality, moment of inertia about the spherical center, and particle rotation angle, respectively. For a solid sphere, there is $I = 2mR^2/5$. The rebound angular velocity, tangential restitution coefficient, and the rebound translational velocities at the contact path can be written as

$$\omega_r = \omega_i - \frac{5(V_{ti} - V_{tr})}{2R} = \omega_i - \frac{5f(1 + e_n)V_{ni}}{2R} \tag{10}$$

$$e_t = 1 - \frac{f(1 + e_n)}{\tan\theta_i} = 1 + \frac{2R(\omega_r - \omega_i)}{5V_{ni}\tan\theta_i} \tag{11}$$

$$v_{tr} = V_{tr} + R\omega_r = v_{ti} + \frac{7}{5}R(\omega_r - \omega_i) \tag{12}$$

The dimensionless method is introduced to analyze the oblique impact process. The dimensionless rebound angular velocity Φ_r, incident angular velocity Φ_i, the dimensionless rebound tangential surface velocity at the contact path Λ_r, and the dimensionless impact angle Θ are defined as follows[35]

$$\Phi_r = \frac{2R}{5(1 + e_n)\mu_f V_{ni}}\omega_r \tag{13}$$

$$\Phi_i = \frac{2R}{5(1 + e_n)\mu_f V_{ni}}\omega_i \tag{14}$$

$$\Lambda_r = \frac{2}{(1 + e_n)\mu_f V_{ni}}v_{tr} \tag{15}$$

$$\Theta = \frac{2}{(1 + e_n)\mu_f}\tan\theta_i \tag{16}$$

where R is the particle radius and μ_f is the dynamic friction coefficient. Hence, eqs 10−12 can be rewritten as

$$\Phi_r = \Phi_i - \frac{f}{\mu_f} \tag{17}$$

$$e_t = 1 + \frac{2(\Phi_r - \Phi_i)}{\Theta} = 1 - \frac{2f}{\Theta\mu_f} \tag{18}$$

$$\Lambda_r = \Theta + 7\Phi_r - 2\Phi_i = \Theta + 5\Phi_i - \frac{7f}{\mu_f} \tag{19}$$

From eqs 17−19, parameters Φ_r, e_t, and Π_r are functions of Φ_i and Θ. When f/μ_f is determined, the parameters Φ_r, e_t, and Λ_r can be obtained.

4. RESULTS AND DISCUSSION

4.1. Effect of Impact Angle on the Restitution Coefficient. The restitution coefficient is used to determine the energy loss during a collision, which is defined as the ratio of the rebound velocity to the incident velocity. Figure 5 shows

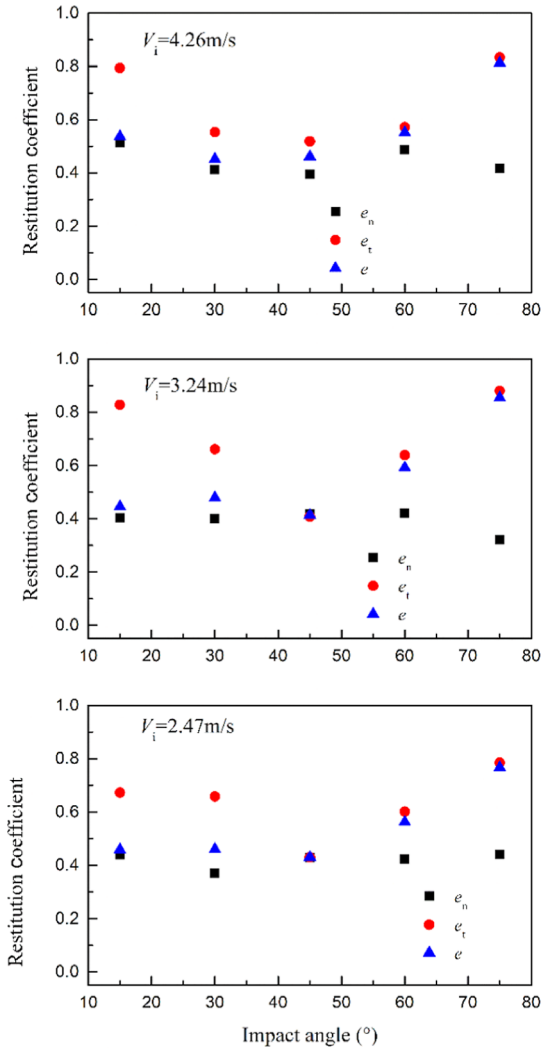

Figure 5. Restitution coefficient versus impact angle at different incident velocities.

the variation of e_n, e_t, and e with the impact angle under the incident velocities of 4.26, 3.24, and 2.47 m/s. The deviation of the incident velocity is ±0.05 m/s. The error bars are not indicated in the graph for clarity. In this experiment, the maximum error of restitution coefficient is less than 10%. As the impact angle increases, the incident kinetic energy is converted into friction and rolling losses. The e_n fluctuates between 0.35 and 0.45 and tends to be constant when the impact angle increases to 45°.

This variation of e_n is inconsistent with the single normal impact process. During oblique impact, the similar regulation of e_n has been obtained by.[10,36] The reason is that only a vertical contact displacement exists between the particles and

https://doi.org/10.1021/acsomega.3c08519
ACS Omega 2024, 9, 10459−10467

the contact surface during normal collisions. The maximum normal contact displacement δ_n is reached. For oblique collisions, however, sliding and rolling occurs between the two contacting surfaces.[21,22] The contact surface changes constantly. Then, the maximum normal contact displacement δ_{on} in an oblique collision does not reach δ_n in a normal collision. The normal energy dissipation is a positive correlation with the maximum normal contact displacement.[37] Therefore, e_n in an oblique collision is larger than that in a normal collision. The energy dissipation can be divided into viscoelastic and plastic deformation losses between the contact surfaces.[38] e_n is not linearly related to the normal incident velocity but remains constant during the viscoelastic loss stage. Consequently, the variation of e_n is small in the experiment.

The trend of e_t decreases first and then increases with the increasing impact angle. At 45°, e_t reaches a minimum of 0.412 at an incident velocity of 2.47 m/s in the experiment. When the impact angle is larger than 45°, e_t increases with increasing impact angle. This is because the tangential kinetic energy increases and the normal load decreases. Therefore, the frictional losses decrease and e_t rises.

The variation of e decreases and then increases with the increasing impact angle. At a low impact angle, e is close to e_n. As impact angle increases, e tends to e_t, which corresponds to eq 5.

4.2. Effect of Impact Angle on Rebound Angle. The rebound angle-particle center θ_r is shown in Figure 6, which is defined as

$$\tan\theta_r = \frac{e_t}{e_n}\tan\theta_i \tag{20}$$

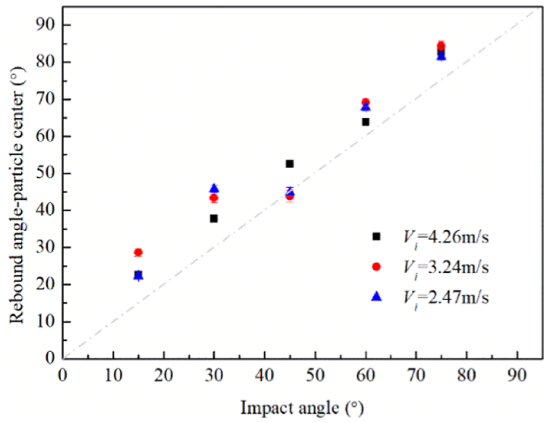

Figure 6. Rebound angle-particle center vs impact angle at different incident velocities.

θ_r increases and is greater than the impact angle as the impact angle increases. For different incident velocities, the difference between rebound angles is small.

The reflection angle-contact path is hard to obtain directly through experiments, which is calculated from experimental data. $\tan\theta_{cr}$ (see Appendix) is calculated as

$$\tan\theta_{cr} = \frac{7e_t - 5}{2e_n\cot\theta_i} \tag{21}$$

θ_{cr} first decreases and then increases with increasing impact angle, as shown in Figure 7. When the impact angle is less than 60°, θ_{cr} is almost less than zero. At 75°, θ_{cr} is positive and

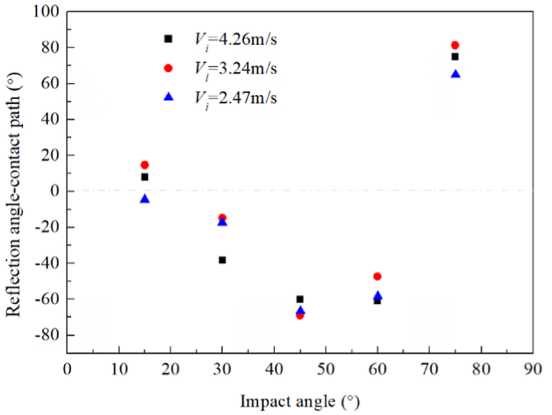

Figure 7. Reflection angle-contact path vs impact angle at different incident velocities.

increases rapidly. The slipping state reduces the friction loss during a collision, which makes e_t and e increase.

4.3. Dynamic Friction Coefficient. During an oblique collision, slipping will cause friction. There is a critical incident angle α_i ($\alpha_i = 90° - \theta_i$) below which a particle in the collision process is the gross slipping state, otherwise it is in the rolling state.[21,22] The dynamic friction coefficient μ_f in tangential force $F_t = \mu_f F_n$ is defined as

$$e_t = 1 - \mu_f\frac{1 + e_n}{\tan\theta_i} \tag{22}$$

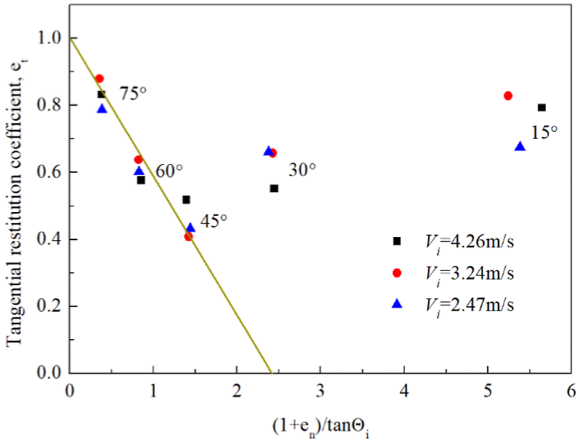

Figure 8. Tangential restitution coefficient versus $(1 + e_n)/\tan\Theta_i$ at different incident velocities.

Figure 8 illustrates the e_t versus $\frac{1+e_n}{\tan\theta_i}$, and the slope of the curve represents the dynamic friction coefficient. In the experiment, the dynamic friction coefficient is 0.417. When the impact angle is greater than 45°, the experimental values are in good agreement with the diagonal line, which indicates that the whole collision process is in a gross slipping state.

4.4. Predictions of Rebound Characteristics of Oblique Impact. *4.4.1. SiO_2 Particles.* The variation of f/μ_f with dimensionless impact angle Θ from Figure S3 is obtained. The dynamic friction coefficient μ_f is a constant that is calculated in Section 4.3. The impulse ratio f increases with the

https://doi.org/10.1021/acsomega.3c08519
ACS Omega 2024, 9, 10459−10467

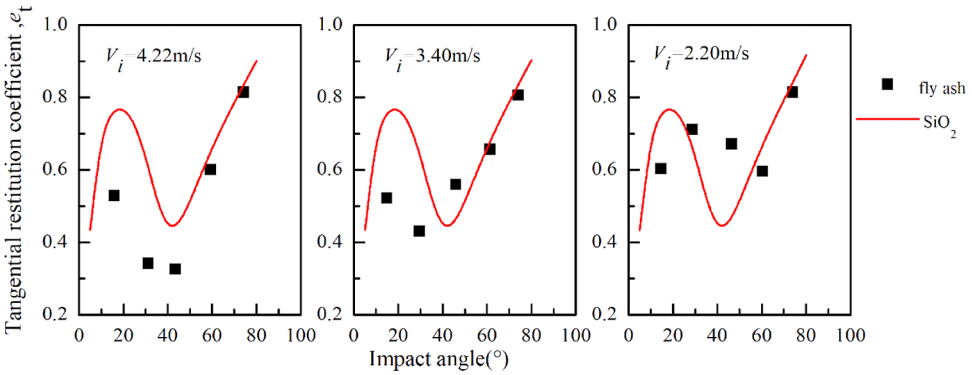

Figure 9. Comparation of the tangential restitution coefficient of SiO_2 and ash particles vs impact angle.

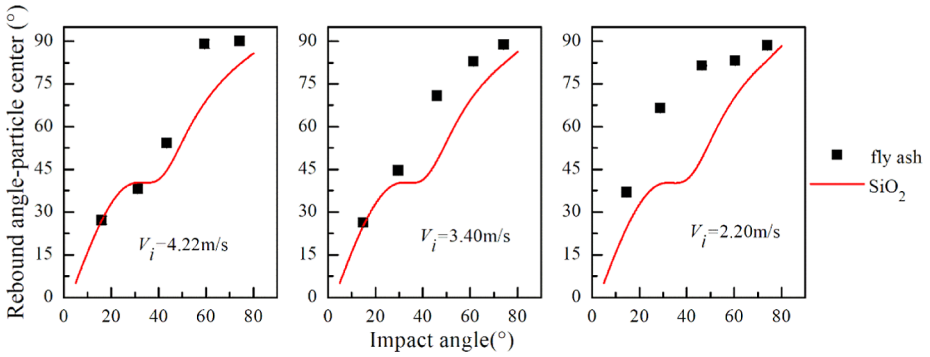

Figure 10. Comparation of the rebound angle-particle center of SiO_2 and ash particles versus the impact angle.

dimensionless impact angle Θ until reaching a certain value. The fitting curve introduces a hyperbolic tangent function, which is expressed as

$$f/\mu_f = 0.448 - 0.602 \tanh(1.023 - 0.451\Theta) \quad (23)$$

When f/μ_f is 1, the particles are grossly sliding from the beginning of contact with the plate to leaving the plate. As the dimensionless impact angle increases, the deviation among the three sets becomes significant. With the increasing impact angle, the shooting process becomes more challenging due to the increased proportion of the flat surface in the captured image. The location of impact on the flat surface exhibits a greater degree of randomness. Therefore, the deviation between the three sets of experimental data from the fitting curve increases.

The critical dimensionless impact angle Θ_c of complete sliding is defined as follows[35,39]

$$\Theta_c = \frac{7\kappa - 1}{\kappa} \quad (24)$$

$$\kappa = \frac{\frac{1-\upsilon_1}{G_1} + \frac{1-\upsilon_2}{G_2}}{\frac{1-\upsilon_1/2}{G_1} + \frac{1-\upsilon_2/2}{G_2}} \quad (25)$$

where G is the shear modulus and υ is the Poisson's ratio. Subscripts 1 and 2 are for the particle and stainless-steel plate, respectively. The critical dimensionless impact angle Θ_c is 5.855. The ratio of f/μ_f reaches a critical value with the increasing dimensionless impact angle Θ. The critical dimensionless impact angle calculated by eq 23 is 5.749°. In contrast to Θ_c obtained by eq 24, the error is 1.81%.

When ignoring the incident angular velocity, the parameters for the rebound characteristics of SiO_2 particles by eqs 17−19 are as follows

$$\Phi_r = \begin{cases} -0.448 + 0.602 \tanh(1.023 - 0.451\Theta) & (\Theta < \Theta_c) \\ -1 & (\Theta \geq \Theta_c) \end{cases} \quad (26)$$

$$e_t = \begin{cases} 1 - 2[0.448 - 0.602 \tan h(1.023 - 0.451\Theta)]/\Theta & (\Theta < \Theta_c) \\ 1 - 2/\Theta & (\Theta \geq \Theta_c) \end{cases} \quad (27)$$

$$\Lambda_r = \begin{cases} \Theta - 7[0.448 - 0.602 \tan h(1.023 - 0.451\Theta)] & (\Theta < \Theta_c) \\ \Theta - 7 & (\Theta \geq \Theta_c) \end{cases} \quad (28)$$

The dimensionless rebound angle velocities (Φ_r) versus the impact angle from G4 are illustrated. During an oblique collision, the tangential force is opposite to the movement of the particles. Therefore, the minus sign indicates the direction. The absolute value of dimensionless rebound angle velocities increases with the increase in incident velocity. When the impact angle is greater than the critical value, Φ_r is constant. The rebound angle velocity will not increase indefinitely. Particles with large velocities have greater inertia and shorter contact times;[10] thus, Φ_r decreases.

The tangential restitution coefficient versus impact angle from G5 is shown. When the impact angle is less than 15°, e_t increases. With increasing impact angle, e_t decreases and then

https://doi.org/10.1021/acsomega.3c08519
ACS Omega 2024, 9, 10459−10467

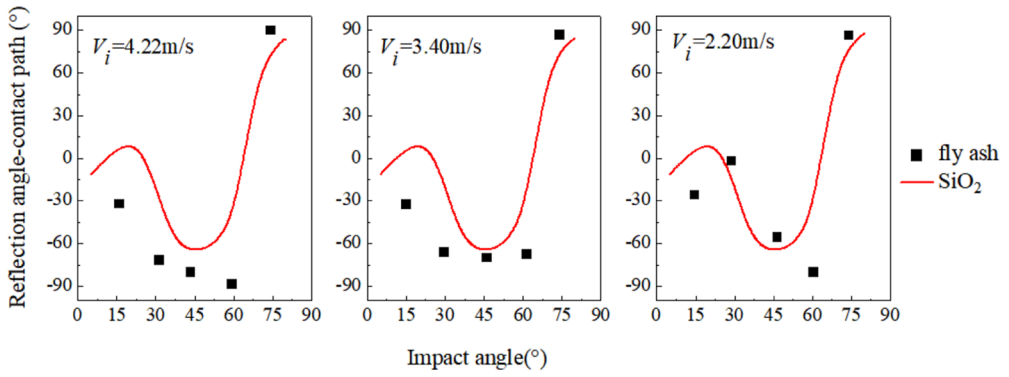

Figure 11. Comparation of the reflection angle-contact path of SiO_2 and ash particles vs impact angle.

increases, reaching the minimum value of 0.431. e_t shows a delay with increasing incident velocity. The larger the incident velocity is, the larger the impact angle corresponding to the minimum e_t. The range of impact angles is 15−75° in the experiment. The variation of e_t in Section 4.1 conforms to this pattern.

4.4.2. Prediction of Ash Particles. Figure 9 shows the tangential restitution coefficient versus impact angle. e_t of SiO_2 can be roughly predicted by the e_t of ash particles. At an incident velocity of 2.2 m/s, the difference in e_t is more obvious. This is because the restitution coefficients fluctuate more as the velocity approaches the critical capture velocity. As the incident velocity increases, e_t fits well, especially at large impact angles. The e is closer to e_t at large impact angles, as shown in Figure 5. Therefore, the total energy loss is in the tangential direction. By comparison of the physical properties of SiO_2 and ash particles, the main difference is Young's modulus. Young's modulus reflects the ability to resist elastic deformation; thus, the larger the value of Young's modulus, the more the energy loss. Therefore, e_t of ash particles is lower than e_t of SiO_2 at speeds of 3.4 and 4.22 m/s. In order to obtain better fitting results, justification is provided by correcting the physical parameters of e_n in the dimensionless impact angle, as shown in eq 16.

Figures 10 and 11 illustrate rebound angle-particle center and reflection angle-contact path versus impact angle, respectively. At 2.2 m/s, the differences between θ_r and θ_{cr} for SiO_2 and ash particles are large, but the overall trends are more similar and can better predict the movement of the particles. At small impact angles, θ_r fit well. Since positive and negative impact angles indicate direction, θ_r and θ_{cr} of ash particles are much larger. This is because of the low sphericity of the ash particles and therefore the large rebound angular dispersion.

5. CONCLUSIONS

An experimental study was performed using SiO_2 and ash particles that obliquely impact the stainless-steel surface under different incident velocities. The rebound behavior of SiO_2 and ash particles was compared by the rigid-body theory. This led to the following conclusions:

(1) In the impact angle range from 15 to 75°, the normal restitution coefficient fluctuates between 0.35 and 0.45 under different incident velocities. As the tangential contact changes from rolling to sliding, the tangential restitution coefficient decreases first and then increases with a minimum impact angle of 45° in the experiment.

(2) The rebound angle-particle center is always larger than the impact angle. At impact angle of 75°, the reflection angle-contact path grows rapidly and greater than 0, which is due to the gross slipping between two contacting surfaces. The dynamic friction coefficient between SiO_2 particles and the stainless-steel surface is 0.417.

(3) By comparison of experimental with theoretical predictions, SiO_2 particles can basically replace ash particles, especially at large impact angles. Except for the slight error at a 2.2 m/s incident velocity, the tangential restitution coefficient, rebound angle-particle center, and reflection angle-contact path are well fitted to the experiment.

■ ASSOCIATED CONTENT

Supporting Information

The Supporting Information is available free of charge at https://pubs.acs.org/doi/10.1021/acsomega.3c08519.

Formula derivation of tan θ_{cr} from the Appendix (PDF)

Diameter distribution of the SiO_2 particles, the images of particle collision, f/μ_f versus Θ at different incident velocities, dimensionless rebound angle velocities versus the impact angle, and tangential restitution coefficient versus impact angle (PDF)

■ AUTHOR INFORMATION

Corresponding Author

Jun Xie − *College of Energy and Environment, Shenyang Aerospace University, Shenyang 110136, China;* orcid.org/0000-0002-3262-0488; Phone: +86-0411-84762312; Email: xiejun@sau.edu.cn; Fax: +86-0411-84762312

Authors

Xue Li − *School of Optical Information and Energy Engineering, Wuhan Institute of Technology, Wuhan 430205, China*

Ming Dong − *School of Energy and Power Engineering, Key Laboratory of Ocean Energy Utilization and Energy Conservation of Ministry of Education, Dalian University of Technology, Dalian 116024, China*

Sheng Chen − *State Key Laboratory of Coal Combustion, School of Energy and Power Engineering, Huazhong University of Science and Technology, Wuhan 430074, China;* orcid.org/0000-0003-0006-973X

https://doi.org/10.1021/acsomega.3c08519
ACS Omega 2024, 9, 10459−10467

Wenjie Dong − *School of Optical Information and Energy Engineering, Wuhan Institute of Technology, Wuhan 430205, China*

Complete contact information is available at: https://pubs.acs.org/10.1021/acsomega.3c08519

Notes

The authors declare no competing financial interest.

■ ACKNOWLEDGMENTS

The authors acknowledge the Foundation of State Key Laboratory of Coal Combustion (no. FSKLCCA2209), Foundation of Wuhan Institute of Technology (no. K2021079), Key Laboratory of Advanced Reactor Engineering and Safety, Ministry of Education (no. ARES202104), and National Natural Science Foundation of China (no: 12302335).

■ REFERENCES

(1) Tang, C.; Pan, W.; Zhang, J.; Wang, W.; Sun, X. A comprehensive review on efficient utilization methods of High-alkali coals combustion in boilers. *Fuel* **2022**, *316*, 123269.
(2) Mendes, L. J.; Bazzo, E.; Toste Azevedo, J. Thermal conductivity analysis of an ash deposit on boiler superheater. *Powder Technol.* **2017**, *318*, 329−336.
(3) Zhu, J. T.; Sun, H. S.; Ren, W. X.; He, X. J.; Wang, L.; Yang, Y. L.; Shi, G. Q. Emission characterization of particulate matters from the combustion of pulverized coals in a simulated fluidized bed boiler. *ACS Omega* **2022**, *7*, 37922−37932.
(4) Huang, Q.; Zhang, Y. Y.; Yao, Q.; Li, S. Q. Numerical and experimental study on the deposition of fine particulate matter during the combustion of pulverized lignite coal in a 25 kW combustor. *Powder Technol.* **2017**, *317*, 449−457.
(5) Bahramian, A.; Olazar, M. Influence of restitution and friction coefficients on the velocity field of polydisperse TiO_2 agglomerates in a conical fluidized bed by the adhesive CFD-DEM simulation. *Powder Technol.* **2021**, *386*, 491−504.
(6) Losurdo, M.; Spliethoff, H.; Kiel, J. Ash deposition modeling using a visco-elastic approach. *Fuel* **2012**, *102*, 145−155.
(7) Xiaoxue, J.; Shuyan, W.; Qinghong, Z.; Baoli, S.; Huilin, L. Granular restitution coefficient-based kinetic theory computations of bubbling fluidized beds. *Powder Technol.* **2021**, *394*, 825−837.
(8) Dodds, D.; Sarhan, A. A. R.; Naser, J. Experimental and numerical study of free-falling streams of particles impacting an inclined surface. *Exp. Comput. Multiph. Flow.* **2023**, *5*, 381−395.
(9) Wang, T. Y.; Ma, L. J.; Wang, M. Y.; Li, Z.; Zhang, X.; Geng, H. S. Effects of particle shape on dynamic mechanical behaviours of coral sand under one-dimensional compression. *Eng. Geol.* **2022**, *304*, 106624.
(10) Xie, J.; Zhu, Z. R.; Yang, T. H.; Dong, M.; Li, R. D. The effect of incident angle on the rebound behavior of micro-particle impacts. *J. Aerosol Sci.* **2021**, *155*, 105778.
(11) Chen, P. Z.; Chen, S.; Wu, T. Y.; Ruan, X.; Li, S. Q. Deposition velocity of inertial particles driven by wall-normal external force in turbulent channel flow. *Phys. Rev. Fluids* **2022**, *7*, 104301.
(12) Dahneke, B. The capture of aerosol particles by surfaces. *J. Colloid Interf. Sci.* **1971**, *37*, 342−353.
(13) Rogers, L. N.; Reed, J. The adhesion of particles undergoing an elastic-plastic impact with a surface. *J. Phys. D* **1984**, *17*, 677−689.
(14) Wall, S.; John, W.; Wang, H. C.; Goren, S. L. Measurements of kinetic energy loss for particles impacting surfaces. *Aerosol Sci. Technol.* **1990**, *12*, 926−946.
(15) Li, X.; Dunn, P. F.; Brach, R. M. Experimental and numerical studies of microsphere oblique impact with planar surfaces. *J. Aerosol Sci.* **2000**, *31*, 583−594.
(16) Li, S. Q.; Marshall, J. S. Discrete element simulation of micro-particle deposition on a cylindrical fiber in an array. *J. Aerosol Sci.* **2007**, *38*, 1031−1046.
(17) Goldsmith, W.; Frasier, J. T. Impact: The theory and physical behavior of colliding solids. *J. Appl. Mech.* **1961**, *28*, 639.
(18) Wu, C. Y.; Thornton, C.; Li, L. Y. Coefficients of restitution for elastoplastic oblique impacts. *Adv. Powder Technol.* **2003**, *14*, 435−448.
(19) Wu, C. Y.; Thornton, C.; Li, L. Y. Rebound behaviour of spheres during elastic-plastic oblique impacts. *Int. J. Mod. Phys. B* **2008**, *22*, 1095−1102.
(20) Tomar, V.; Bose, M. Anomalies in normal and oblique collision properties of spherical particles. *Powder Technol.* **2018**, *325*, 669−677.
(21) Maw, N.; Barber, J. R.; Fawcett, J. N. The oblique impact of elastic spheres. *Wear* **1976**, *38*, 101−114.
(22) Maw, N.; Barber, J. R.; Fawcett, J. N. The role of elastic tangential compliance in oblique impact. *J. Lubrication Technol.* **1981**, *103*, 74−80.
(23) Troiano, M.; Solimene, R.; Salatino, P.; Montagnaro, F. Multiphase flow patterns in entrained-flow slagging gasifiers: Physical modelling of particle-wall impact at near-ambient conditions. *Fuel Process. Technol.* **2016**, *141*, 106−116.
(24) Chen, H.; Pan, P. Y.; Wang, Y. G.; Zhao, Q. X. Field study on the corrosion and ash deposition of low-temperature heating surface in a large-scale coal-fired power plant. *Fuel* **2017**, *208*, 149−159.
(25) Ito, M.; Horiguchi, G.; Hariu, T.; Ito, A.; Kamiya, H.; Okada, Y. Controlling fly ash adhesion at high temperatures via porosity effect. *Powder Technol.* **2020**, *374*, 492−495.
(26) Tomeczek, J.; Wacławiak, K. Two-dimensional modelling of deposits formation on platen superheaters in pulverized coal boilers. *Fuel* **2009**, *88*, 1466−1471.
(27) Yang, X.; Ingham, D.; Ma, L.; Troiano, M.; Pourkashanian, M. Prediction of particle sticking efficiency for fly ash deposition at high temperatures. *Proc. Combust. Inst.* **2019**, *37*, 2995−3003.
(28) Troiano, M.; Santagata, T.; Montagnaro, F.; Salatino, P.; Solimene, R. Impact experiments of char and ash particles relevant to entrained-flow coal gasifiers. *Fuel* **2017**, *202*, 665−674.
(29) Troiano, M.; Solimene, R.; Montagnaro, F.; Salatino, P. Char/ash deposition and near-wall segregation in slagging entrained-flow gasification of solid fuels: from experiments to closure equations. *Fuel* **2020**, *264*, 116864.
(30) Hu, S. H.; Yin, Q.; Zhang, Y. Z.; Cen, K. F.; Zhou, H. Experimental study on the rebound characteristics of oblique collision of ash particles and the influence of ammonium bisulfate. *Aerosol Sci. Technol.* **2022**, *56*, 1058−1069.
(31) Xie, J.; Dong, M.; Li, S. F.; Mei, Y. K.; Shang, Y. An experimental study of fly ash particle oblique impact with stainless surfaces. *J. Aerosol Sci.* **2018**, *123*, 27−38.
(32) Wall, T. F.; Lowe, A.; Wibberley, L. J.; McC Stewart, I. Mineral matter in coal and the thermal performance of large boilers. *Prog. Energ. Combust.* **1979**, *5*, 1−29.
(33) Li, X.; Dong, M.; Li, S. F.; Shang, Y. Experimental and theoretical studies of the relationship between dry and humid normal restitution coefficients. *J. Aerosol Sci.* **2019**, *129*, 16−27.
(34) Liu, X. W.; Xu, M. H.; Yu, D. X.; Yu, Y.; Gao, X. P.; Cao, Q. Research on formation and emission of inhalable particulate matters at different oxygen content during coal combustion. *Proc. Chin. Soc. Electr. Eng.* **2006**, *26*, 45−50.
(35) Wu, C. Y.; Thornton, C.; Li, L. Y. A semi-analytical model for oblique impacts of elastoplastic spheres. *Proc. R. Soc. A: Math. Phys.* **2009**, *465*, 937−960.
(36) Li, X.; Dunn, P. F.; Brach, R. M. Lycopodium spore impacts onto surfaces. *Atmos. Environ.* **2000**, *34*, 1575−1581.
(37) Dong, M.; Li, X.; Mei, Y. K.; Li, S. F. Experimental and theoretical analyses on the effect of physical properties and humidity of fly ash impacting on a flat surface. *J. Aerosol Sci.* **2018**, *117*, 85−99.
(38) Liu, G.; Li, S.; Yao, Q. A JKR-based dynamic model for the impact of micro-particle with a flat surface. *Powder Technol.* **2011**, *207*, 215−223.

(39) Johnson, K. *Contact mechanics*; Cambridge University Press, 1974.

https://doi.org/10.1021/acsomega.3c08519
ACS Omega 2024, 9, 10459−10467